Evaluating Self-Produced PLA Filament for Sustainable 3D Printing: Mechanical Properties and Energy Consumption Compared to Commercial Alternatives

Journal of
Manufacturing and Materials Processing

MDPI

Article

Evaluating Self-Produced PLA Filament for Sustainable 3D Printing: Mechanical Properties and Energy Consumption Compared to Commercial Alternatives

Luca Fontana [1], Paolo Minetola [2,3], Mankirat Singh Khandpur [2,3] and Alberto Giubilini [2,3,*]

[1] Department of Applied Science and Technology (DISAT), Politecnico di Torino, Corso Duca Degli Abruzzi 24, 10129 Torino, Italy; luca.fontana@polito.it
[2] Department of Management and Production Engineering (DIGEP), Politecnico di Torino, Corso Duca Degli Abruzzi 24, 10129 Torino, Italy; paolo.minetola@polito.it (P.M.); mankirat.khandpur@polito.it (M.S.K.)
[3] Integrated Additive Manufacturing Centre (IAM@PoliTO), Politecnico di Torino, Corso Duca Degli Abruzzi 24, 10129 Torino, Italy
* Correspondence: alberto.giubilini@polito.it

Abstract: This study investigates the feasibility of self-producing polylactic acid (PLA) filament for use in 3D printing. The filament was fabricated using a desktop single-screw extruder and evaluated against commercially available PLA in terms of mechanical properties and energy consumption. Specimens were printed at two layer heights (0.2 mm and 0.3 mm) and four infill densities (25%, 50%, 75%, and 100%). The self-produced filament exhibited lower diameter precision (1.67 ± 0.21 mm), which resulted in mass variability up to three orders of magnitude higher than that of the commercial filament. Thermal analysis confirmed that the extrusion and printing process did not significantly alter the thermal properties of PLA. Mechanical testing revealed that a layer height 0.3 mm consistently yielded higher stiffness and tensile strength in all samples. When normalized by mass, the specimens printed with commercial filament demonstrated approximately double the ultimate tensile strength compared to those that used self-produced filament. The energy consumption analysis indicated that a 0.3 mm layer height improved printing efficiency, cutting specific energy consumption by approximately 50% and increasing the material deposition rate proportionally. However, the total energy required to print with self-produced filament was nearly three times higher than that for commercial filament, primarily due to material waste that stems from inconsistencies in the diameter of the filament. These findings are significant in evaluating the practicality of self-produced PLA filament, particularly in terms of mechanical performance and energy efficiency.

Keywords: polylactic acid; additive manufacturing; fused filament fabrication; single-screw extrusion

Academic Editor: Sharifu Ura

Received: 23 April 2025
Revised: 16 May 2025
Accepted: 21 May 2025
Published: 24 May 2025

Citation: Fontana, L.; Minetola, P.; Khandpur, M.S.; Giubilini, A. Evaluating Self-Produced PLA Filament for Sustainable 3D Printing: Mechanical Properties and Energy Consumption Compared to Commercial Alternatives. *J. Manuf. Mater. Process.* **2025**, *9*, 172. https://doi.org/10.3390/jmmp9060172

1. Introduction

Additive manufacturing (AM), commonly known as 3D printing, has emerged as a game-changing technology in various fields of application, ranging from biomedical [1–5] to aerospace [6], motor racing [7,8], and energy storage [9], with polymers being key players in this revolution. Polymer AM diffusion has facilitated the establishment of miniature production clusters, where users actively participate in the production process, exerting a notable influence on the distribution and subsequent flow of materials and goods within the value chain [10]. Manufacturing clusters are designed to minimize production time while enhancing resource efficiency [11]. Among all polymer AM techniques, fused

filament fabrication (FFF) is the most popular methodology, due to its straightforwardness, versatility, and cost-effectiveness. FFF involves a layer-by-layer deposition approach using thermoplastic filaments to manufacture objects with complex three-dimensional geometries [12]. With FFF, the extent of customer integration into the manufacturing process directly impacts the customization level of products, correlating to a significantly more tailored and customized manufacturing experience [13,14].

Currently, the modern manufacturing industry faces a fundamental challenge in addressing environmental issues. In this context, the circular economy plays a crucial role in sustainability efforts, attempting to minimize waste streams and maximize the lifetime of materials [15,16]. From a circular economy perspective, 3D printing has the potential to enhance the use of resources and optimize the value chain of established production methods [17–19]. Senyana et al. suggested that a transition toward decentralized manufacturing highlights the potential of AM technologies to contribute to a sustainable manufacturing system [20]. Moreover, waste parts can be transformed into raw materials for new productions, thereby increasing the recycling of polymer components with reduced costs and environmental impact [21]. For example, FFF is well aligned with this perspective, as it enables the use of recycled or bio-based filaments, thereby reducing the environmental impact associated with polymer production and depletion of fossil sources [22]. Sustainability in AM is integrated across its lifecycle: in design, strategies like topology optimization and part consolidation reduce material use and improve durability; during AM, process monitoring and closed-loop control enhance reliability and energy efficiency; and post-AM, repair, remanufacturing, and recycling extend product lifecycles, aligning with circular economy principles [23].

In the last twenty years, polylactic acid (PLA) has emerged as a popular environmentally friendly thermoplastic polymer for FFF, which can be derived from renewable resources such as corn starch or sugarcane [24–27]. Commercially available PLA filaments are renowned for their ease of use, low odor, minimal warping during printing, wide range of colors, and excellent compatibility with 3D printing. These qualities make them a go-to choice for users seeking a versatile and sustainable material for personal needs or even small industrial applications [28,29]. Beyond its printability, PLA is valued for its biocompatibility and biodegradability, enabling its use in biomedical applications, such as tissue engineering, drug delivery, and medical implants. Its biodegradation through hydrolytic processes results in non-toxic byproducts, highlighting its appeal as a sustainable alternative to petroleum-based polymers [30]. However, PLA's mechanical properties, including tensile and impact strength, are lower than those of other thermoplastic polymers like ABS or PETG, limiting its use in high-stress applications [31]. Its low heat deflection temperature of around 55 °C restricts its suitability for heat-exposed environments, as deformation may occur [32]. Moreover, its degradation rate is influenced by environmental factors, which pose challenges to long-term predictability [33]. These limitations have driven research into polymer blends, copolymers, and composite materials to enhance their thermal and mechanical performance while maintaining their sustainability attributes [34]. Users can autonomously produce polymer filaments directly from pellets using small desktop extruders. This self-produced filament can subsequently serve as a feedstock for FFF [35–38]. A review of previous research papers revealed some interesting advantages and disadvantages associated with self-produced filaments. One of the main benefits is the potential for cost reduction; in fact, for the same amount of material, the average cost of a filament spool is approximately twice that of a pellet [39,40]. By enhancing filament self-production, users can explore locally sourced and recycled materials [41], which aligns with sustainability goals and contributes to the circular economy by reducing dependence on commercially manufactured filaments. More importantly, self-produced filaments offer customization

options, allowing users to tailor the material properties to specific applications by adding, mixing, or blending the polymer matrix with reinforcing or functional materials. For example, polymer matrices reinforced with recycled carbon, basalt, or glass fibers exhibit increased Young's modulus and tensile strength [42–45]. Ceramic components, such as alumina, have been incorporated to develop filaments intended for 3D printing, followed by debinding and sintering to produce end-usable ceramic parts [46]. In the biomedical field, bioactive fillers like hydroxyapatite, tricalcium phosphate, and cellulose nanocrystals have been compounded with various polymer matrices, including PCL, PLGA, PLA, and PHBH, to 3D print scaffolds with enhanced functionalities, such as osteogenic activity, improved cell viability, and angiogenesis [47–50]. Additionally, conductive properties have been imparted to FFF filaments by incorporating carbon-based materials, such as carbon black nanoparticles, graphite, and carbon nanotubes, paving the way for the 3D printing of next-generation sensors [51,52]. However, several challenges remain in using self-produced filaments, including the need for specialized extrusion equipment and the difficulty in achieving a consistent filament diameter comparable to that of commercial filaments. In FFF, the filament material requirements are critical for print quality and mechanical performance. Variability in diameter can cause uneven extrusion, affecting the material flow, layer adhesion, and surface finish. Key extrusion parameters, such as the extrusion temperature, extrusion speed, and cooling rate, must be carefully controlled to maintain consistency [53]. Additionally, controlling the moisture content is essential, particularly for hygroscopic materials like PLA or polyamide (PA), to prevent defects such as bubbling and weak interlayer bonding [54].

This research aims to expand the current knowledge on self-produced polymer filaments for FFF. By analyzing the thermal and mechanical properties of the fabricated samples, the study provides insights into the applicability and performance of a self-produced PLA filament compared to a commercial one. Furthermore, the investigation of the tensile properties of 3D printed samples as a function of infill percentage and layer height, along with energy consumption assessments, offers a better understanding of the production process and its sustainability implications. The use of X-ray computed tomography (X-CT) for cross-sectional area analysis further enhances the study's comprehensiveness. Ultimately, this research aims to shed new light on the potential of self-made filaments as a viable and increasingly desirable alternative to commercial filaments, supporting the advancement of more sustainable and customizable AM solutions.

2. Materials and Methods

2.1. Materials

Polylactic acid (PLA) pellets, identified by the commercial code PLA 3D850, were supplied by Smart Materials 3D (Smart Materials 3D, Jaén, Spain). Before processing, the PLA was dried at 80 °C for 4 h in an oven to eliminate any moisture. A commercial spool of PLA 3D850 filament was supplied by the same company (Smart Materials 3D, Jaén, Spain). 3D850 Natural PLA 3D printing filament was designed using a biodegradable polymer derived from Ingeo^{TM} PLA 3D850 (NatureWorks, Blair, NE, USA).

2.2. Filament Production

Self-produced PLA filament spools were fabricated using a single-screw desktop extruder model NEXT 1.0 (3devo B.V., Utrecht, The Netherlands), as shown in Figure 1a. The extruder was equipped with four heating systems that were installed from the sub hopper to the nozzle. To extrude the pellets of PLA 3D850, the following thermal profile was set along the screw length: 170 °C, 185 °C, 190 °C, and 180 °C (Figure 1b). This temperature profile was initially based on the manufacturer's recommendations for generic PLA and

was then fine-tuned to suit the specific processability of the PLA under investigation, in accordance with the previous processing of these pellets using the same extruder [55]. The first three heating zones were set to progressively increasing temperatures, while the final zone was adjusted to the melting temperature of PLA, as determined by the DSC analysis of the raw pellets. The rotation speed of the screw motor (M) and winding speed were set to be automatically controlled by the extruder to achieve a final desired diameter of 1.75 mm through a feedback system with optical control (OC) of the filament size. The cooling fans (CF) were set to 80%, and the extruder screw speed was set to 4.5 rpm.

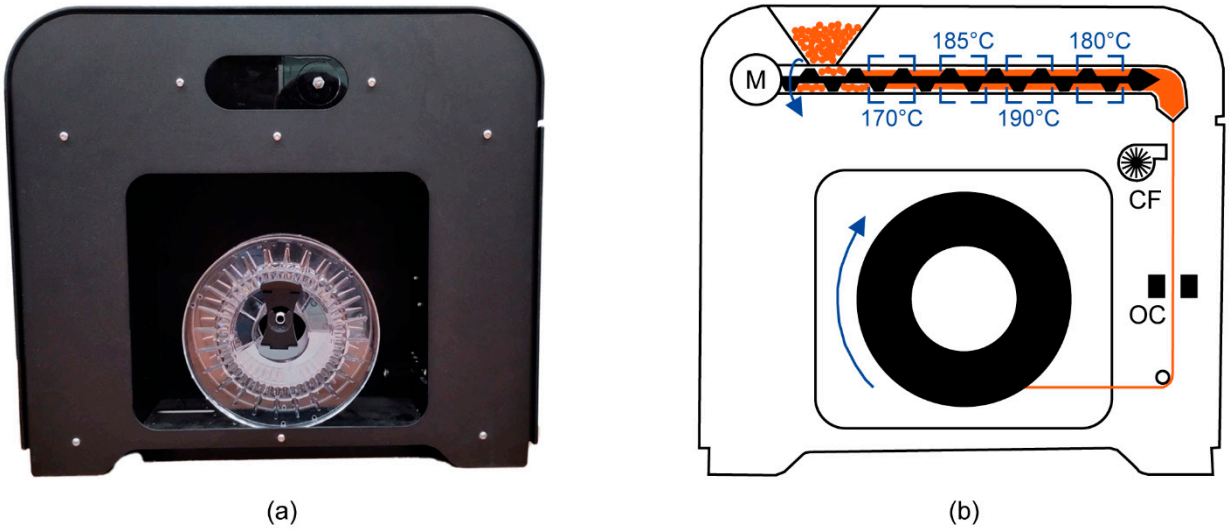

Figure 1. Single-screw desktop extruder by 3devo for self-production of PLA filament: photo of the machine (**a**) and scheme with the main components and temperatures (**b**).

2.3. Samples 3D Printing

Both self-produced and commercial PLA filaments were employed on an Ender 3-Pro (Creality, Shenzhen, China) 3D printer (Figure 2) to fabricate tensile testing specimens, following the ISO 527 standard (type 1BA) [56]. The specimen design (Figure 3) was realized using SolidWorks 2023 CAD software (Dassault Systèmes, Vélizy-Villacoublay, France). The Creality Slicer 4.8.2 software (Creality, Shenzhen, China) was then used to slice the STL file and generate the G-code printing files. Table 1 provides a summary of the main parameters used for 3D printing the specimens.

Table 1. 3D printing parameters of all PLA specimens.

Parameter	Value
Nozzle temperature (°C)	235
Platform temperature (°C)	60
Printing speed (mm/s)	53
Nozzle diameter (mm)	0.4
Infill pattern	Linear
Infill angle (°)	±45
Number of top/bottom layers	3

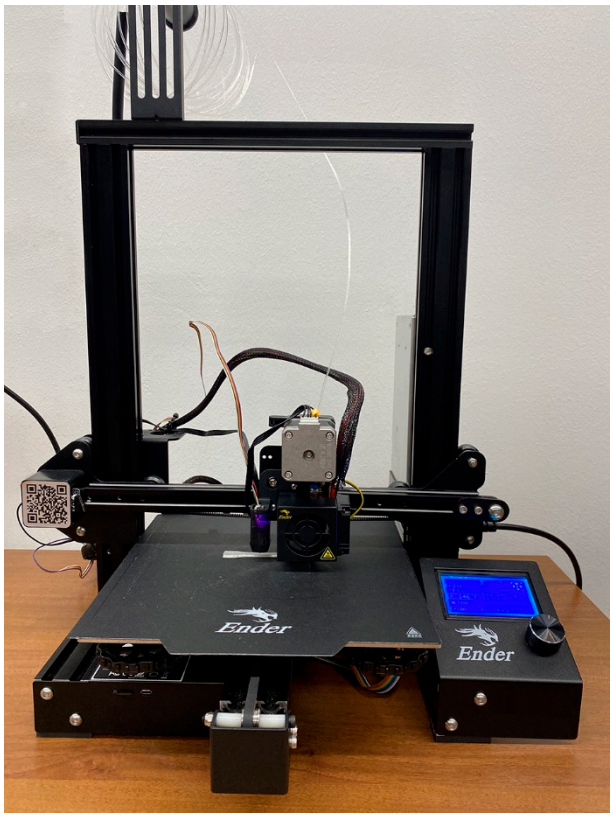

Figure 2. Photograph of the Ender 3-Pro 3D printer.

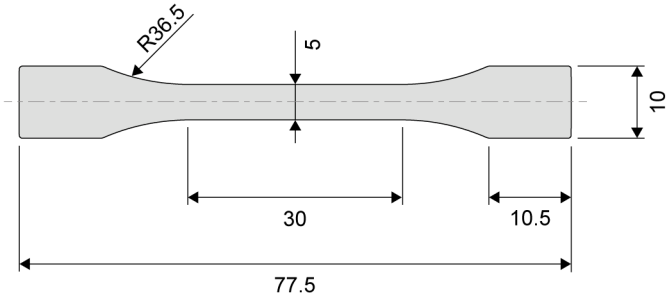

Figure 3. Dimensions of the tensile specimens following the ISO 527 standard for type 1BA [56], with a thickness of 2 mm.

Two different layer heights of 0.2 and 0.3 mm were used at four distinct infill percentages: 25%, 50%, 75%, and 100%. Considering the 2 mm thickness for the type 1BA specimen, 10 layers were printed with a layer height of 0.2 mm, while 7 layers were deposited when adopting a layer height of 0.3 mm.

After production, the specimens were stored under constant environmental conditions of 20 °C and 50% humidity before testing in the tensile machine.

2.4. Characterization Techniques

2.4.1. Optical Microscopy

Magnified details of the filaments were obtained using a Leica S9i (Leica Camera AG, Wetzlar, Germany) stereomicroscope. This microscope offers a maximum magnification of 55× and features an integrated 10-megapixel camera for capturing full-HD (1080p) images.

2.4.2. Energy Consumption

The power consumption during both filament production and 3D printing was measured using a Meterk M34EU power meter plug (Shenzhen Tomtop Technology Co., Ltd., Shenzhen, China). For the 3D printed samples, two additional parameters were calculated to characterize the production process: specific energy consumption (SEC) and deposition rate (DR). SEC is defined as the energy required to 3D print a specimen, normalized by its mass, while DR represents the mass of the specimen divided by the 3D printing time, expressed in grams per hour (g/h). To calculate the SEC value, the secondary energy, i.e., electricity consumption, was used in this work without accounting for energy losses from generation, conversion, and distribution.

2.4.3. Differential Scanning Calorimetry (DSC)

The main thermal properties of both the PLA pellets and 3D printed specimens obtained using the self-produced filament were evaluated using DSC. These experiments were conducted using a DSC 214 Polyma calorimeter (Netzsch Group, Selb, Germany). Two heating scans were performed on 8 mg samples sealed in aluminum trays under a N_2 flow rate of 40 mL/min. The samples were tested using a heating ramp of 10 °C/min from 0 to 250 °C, followed by a cooling ramp of 10 °C/min from 250 to 0 °C. The analysis of the curves determined: the glass transition temperature (T_g), the melting temperature (T_m), the cold crystallization temperature (T_{cc}), the crystallization temperature (T_c), along with their associated enthalpies of fusion (ΔH_m), and cold crystallization (ΔH_{cc}). The degree of crystallinity (X_c) was estimated using Equation (1):

$$X_c(\%) = \frac{\Delta H_m - \Delta H_{cc}}{\Delta H_m^0} \times 100 \quad (1)$$

where ΔH_m^0 is the theoretical melting enthalpy of 100% crystalline PLA, assumed to be 93 J/g [40].

2.4.4. X-Ray Computed Tomography (X-CT)

The cross-sectional area of the 3D printed specimens was analyzed using X-CT with a Phoenix v|tome|x S240 micro-CT system (GE Baker Hughes-Waygate Technologies, Wunstorf, Germany). Because the tensile specimens were long and a voxel size of 29.6 µm was chosen, the multi-scan function of the datos|acquisition v1.3.2 software was used. The other X-ray scan parameters were a voltage of 190 kV, a current of 160 µA, a timing of 100 ms, and 1500 images were acquired for each scan. Following the acquisition of the X-ray images, reconstruction was performed using the datos|reconstruction v2.1.0 software. Subsequently, the reconstructed data were transferred to VG Studio Max software (version 3.4) by Volume Graphics (Hexagon Metrology-Volume Graphics, Heidelberg, Germany) for visualization and analysis. The first step involved the determination of the surface, conducted with the *Advanced (classic)* approach, starting the contour from the histogram with an *Automatic* material definition. This method performs segmentation by transforming 3D voxel data into 3D surface data by identifying the interfaces between solid materials and the surrounding air or between different solid materials. The VG Studio Max software assigns a gray threshold value to the edge voxels to achieve surface determination.

2.4.5. Tensile Testing

For each layer height and infill percentage, 5 specimens were 3D printed from the self-produced filament and 3 from the commercial spool using an Aura 5T machine (Easydur, Arcisate, Italy) following the UNI ISO 527 standard [57]. The machine was equipped with a 5 kN load cell, and a crosshead speed of 5 mm/min was set during the tensile tests, in

accordance with the referenced standard. The calculation of strain at break (ε_b), ultimate tensile strength (UTS), and Young's modulus (E) was performed using the obtained stress-strain curves. Before testing, all samples were weighed using a Gibertini balance (Gibertini, Novate Milanese, Italy), and their average thickness and width were measured using a caliper.

3. Results and Discussion

3.1. Filament Production and 3D Printing Samples

The diameter of the filament plays a significant role in the 3D printing process; therefore, the first analysis conducted was aimed at determining the consistency of the produced filament in relation to its average diameter and production yield. The production yield parameter was calculated as the percentage ratio between the mass of pellets initially inserted in the hopper (170 g) and the mass of usable filament produced (130 g), excluding filament segments with improper diameters, i.e., exceeding 1.9 mm or smaller than 1.4 mm. Over a total filament length of 72 m, the diameter of the self-produced filament was measured using a micrometer in 222 positions, corresponding to about one value every 350 mm. Figure 4 shows the distribution of the diameter values of the self-produced filament.

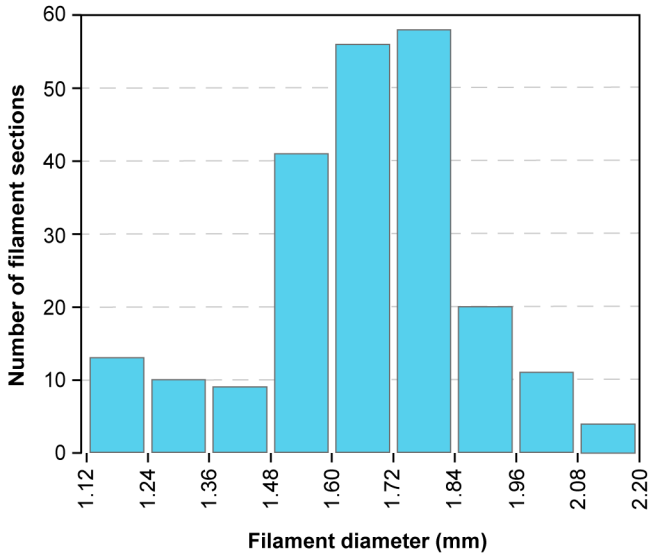

Figure 4. Distribution of the diameter values at 222 positions over the total extruded length of 72 m for the self-produced filament.

In 54 transversal sections, the filament diameter fell outside the range of 1.4 mm to 1.9 mm. This calculation resulted in a final production efficiency of 76.5%, indicating that approximately one-quarter of the material was discarded due to excessive deviations from the target diameter value of 1.75 mm. This high variability was also observed in the calculation of the average filament diameter. Including the most discordant portions, the average diameter of the extruded filament was 1.67 $\pm$ 0.21 mm over a total length of 72 m. Although this value does not match the precision of commercially available filaments, which are typically around 1.75 $\pm$ 0.05 mm, it is consistent with other experimentally produced filaments. For example, Andersson et al. fabricated a PLA-based filament using a 3devo extruder with a diameter of 1.50 $\pm$ 0.10 mm [58].

Figure 5 presents and compares two views of segments from distinct filaments: the commercial PLA 3D850 filament (a1) and (b1) and the self-produced filament (a2), (a3), (b2), and (b3). The former filament exhibits a flawless circular cross-section, while the self-produced filament displays both regular portions and others with a more irregular

cross-section. These irregularities might be ascribed to the compression of the filament between the wheels of the filament pulling and winding system in the 3devo extruder or an inconsistent extrusion flow rate.

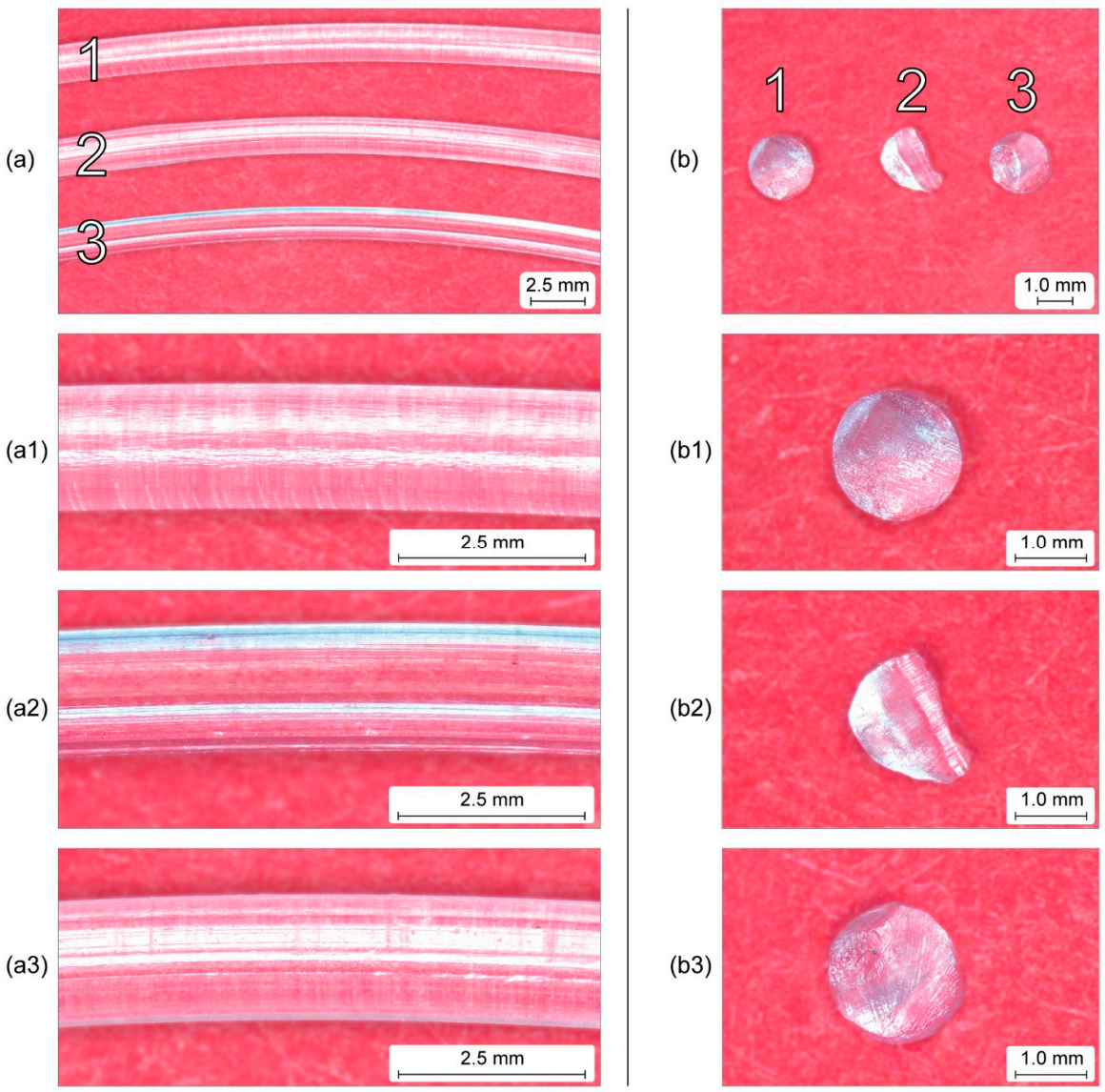

Figure 5. Optical microscopy images of the top view (**a**) and cross-section (**b**) of commercially available PLA (**a1**,**b1**), flattened shape of the self-produced PLA filament (**a2**,**b2**), and circular shape of the self-produced PLA filament (**a3**,**b3**).

Previous literature has already identified that the variability in the extruded filament diameter is highly sensitive to process parameters such as processing temperature, feed flow, screw rotation speed, and even the backflow of material in the feeding zone [36,59–61]. Consequently, the final quality of the 3D print is affected by the size and the consistency of the filament. The high variability of the filament diameter may cause an inconsistent flow rate of the extruded and deposited material during 3D printing, which results in imperfections in the printed object [62–64].

Figure 6 shows 3D printed PLA tensile specimens fabricated using the self-produced filament with a layer thickness of 0.3 mm representing both layer heights. For all infill percentages, the top layers are fully dense and thus do not allow for a clear internal view. However, the quality of the samples seems to be only slightly affected by the non-uniformity of the filament diameter.

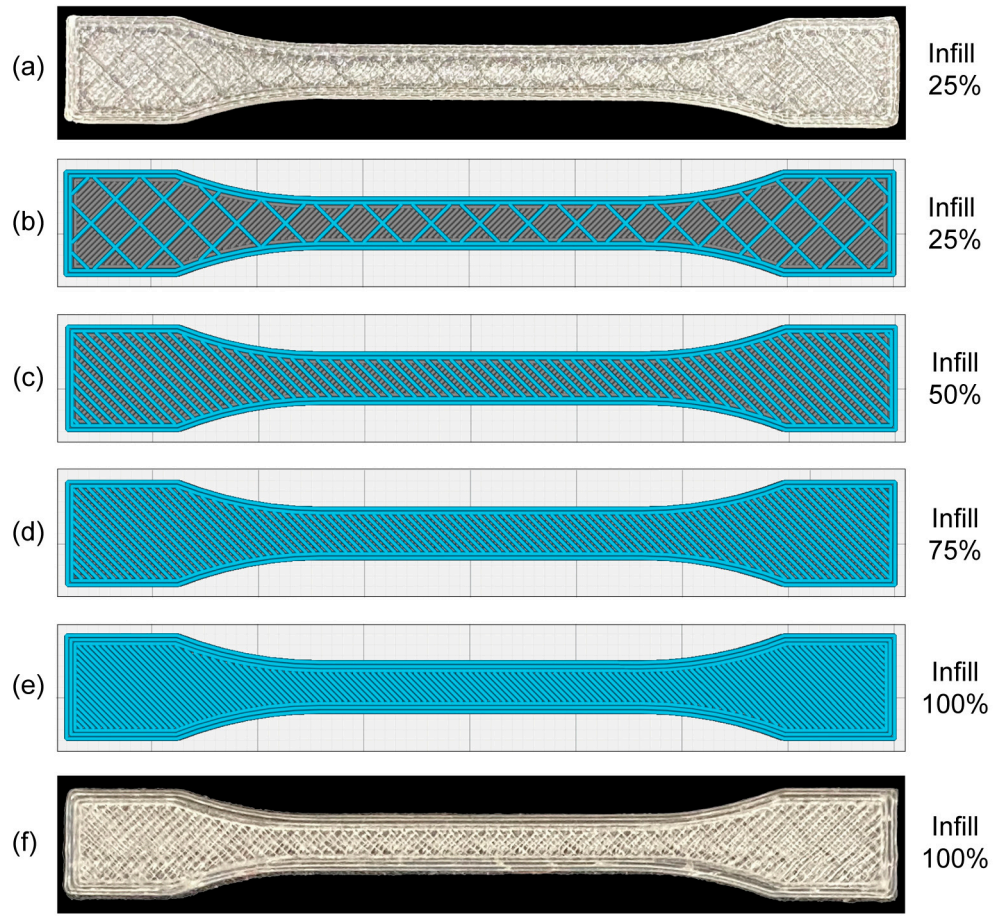

Figure 6. Samples fabricated with self-produced PLA filament and a layer height of 0.3 mm: 3D printed with 25% infill (**a**); printing path for 25% infill (**b**); printing path for 50% infill (**c**); printing path for 75% infill (**d**); printing path for 100% infill (**e**); 3D printed with 100% infill (**f**).

Nevertheless, the quality observed through visual inspection and specimen aesthetics is not confirmed by the analysis of the distribution of the sample mass. The masses of the tensile specimens 3D printed using the self-produced PLA filament are summarized in Table 2.

Table 2. Mass of the tensile specimens 3D printed using the self-produced PLA filament classified according to the layer height and infill percentage.

Layer Height (mm)	**0.2**				**0.3**			
Infill Percentage (%)	**25**	**50**	**75**	**100**	**25**	**50**	**75**	**100**
Mass of specimen 1 (g)	0.653	0.775	1.018	1.360	1.091	1.170	1.305	1.440
Mass of specimen 2 (g)	0.645	0.762	0.940	1.206	1.071	1.129	1.164	1.239
Mass of specimen 3 (g)	0.646	0.744	0.912	0.987	1.028	1.150	1.219	1.277
Mass of specimen 4 (g)	0.645	0.803	0.880	0.960	1.044	1.043	1.188	1.241
Mass of specimen 5 (g)	0.662	0.756	0.835	0.987	1.060	1.163	1.258	1.289
Mean value (g)	0.650	0.768	0.917	1.100	1.059	1.131	1.227	1.297
Standard deviation (g)	0.007	0.023	0.069	0.176	0.024	0.052	0.056	0.083

The average mass of the corresponding specimens with the same infill percentage is higher for the larger layer height because more material is deposited in each layer. For the same layer thickness, as the infill percentage increases, the average mass of the specimen also increases because more extruded filament is deposited in each cross-sectional layer.

Notably, the mass varies significantly between the specimens printed with the minimum and maximum infill, with a difference of 69% for a layer height of 0.2 mm and 22% for a layer height of 0.3 mm. Moreover, with an increase in the infill percentage, the standard deviation associated with the mass of the five specimens per type also increases. This result confirms that the variation in filament diameter might affect the variability of the flow rate during the extrusion in 3D printing. An inconsistent flow rate results in higher variability in the deposited mass for those specimens that are printed with larger infill percentages.

3.2. Energy Consumption

To further characterize the 3D printing process of the different samples, an analysis of the energy consumption was conducted. Figure 7 depicts the key findings, highlighting the influence of the layer height and infill percentage on the SEC and DR. The analysis revealed that samples 3D printed with a 0.2 mm layer height, represented by the blue dashed-line cluster on the left in Figure 7, exhibited higher SEC and lower DR on average, with a centroid positioned at about 86 MJ/kg and 5 g/h. Conversely, samples 3D printed with a layer height of 0.3 mm, represented by the red dashed-line cluster on the right in Figure 7, demonstrated a lower SEC and higher DR, with a centroid placed at around 38 MJ/kg and 8.6 g/h. These findings indicate that using a higher layer height is more energy-efficient and allows for greater productivity. Additionally, within the 0.2 mm layer height cluster, increasing the infill percentage resulted in a decreasing SEC trend. For samples with a layer height of 0.3 mm, increasing the infill percentage shifts the DR toward higher values. These observations align with the trends reported in previous studies [65,66], reinforcing the understanding of how printing parameters affect energy efficiency and deposition performance. The data for the energy consumption analysis are presented in Tables S1 and S2 in the Supplementary Materials.

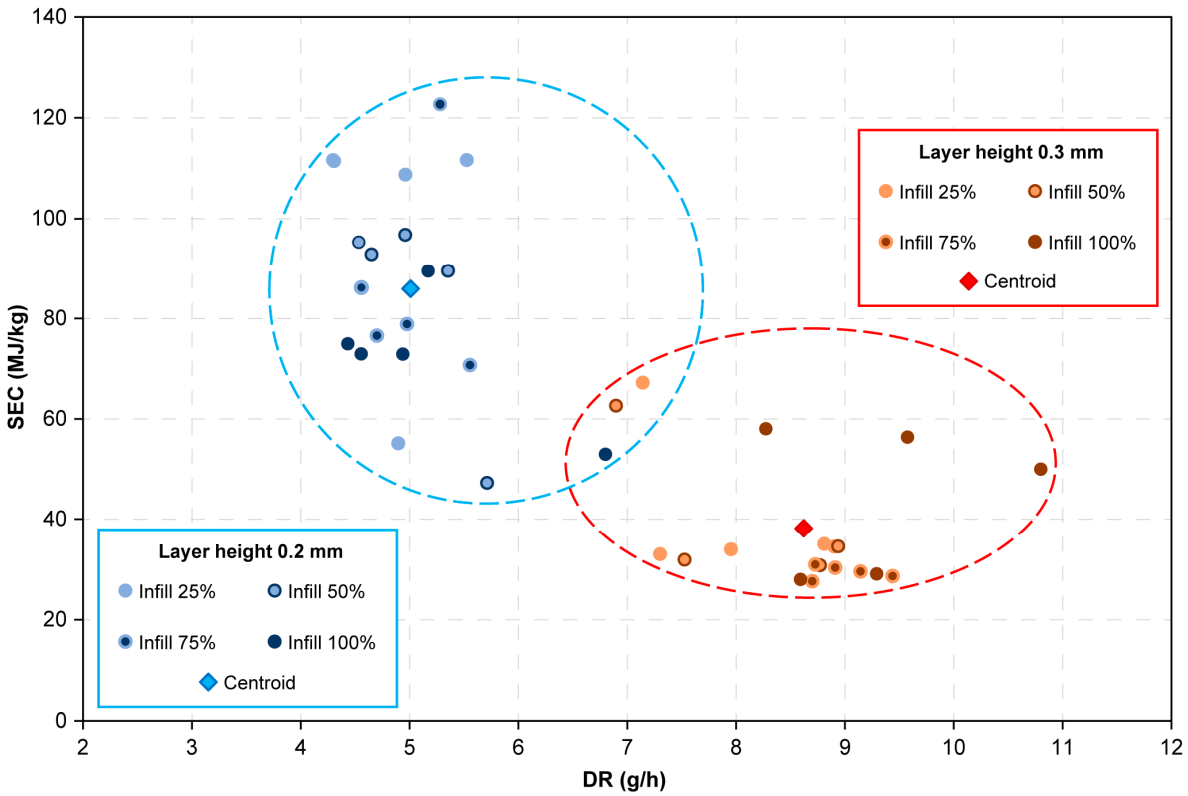

Figure 7. Correlation between the specific energy consumption (SEC) and deposition rate (DR) for the tensile specimens printed with self-produced PLA filament at different layer heights and infill percentages.

3.3. Thermal Characterization

To thermally characterize the PLA material and determine the impact of filament self-production and the influence of 3D printing on the PLA structure and properties, three different DSC scans were performed on unprocessed PLA (Pellet), self-extruded filament (Filament), and a 3D printed sample (3DP sample). Figure 8a,b show the scans for the first heating and cooling of the different samples, respectively.

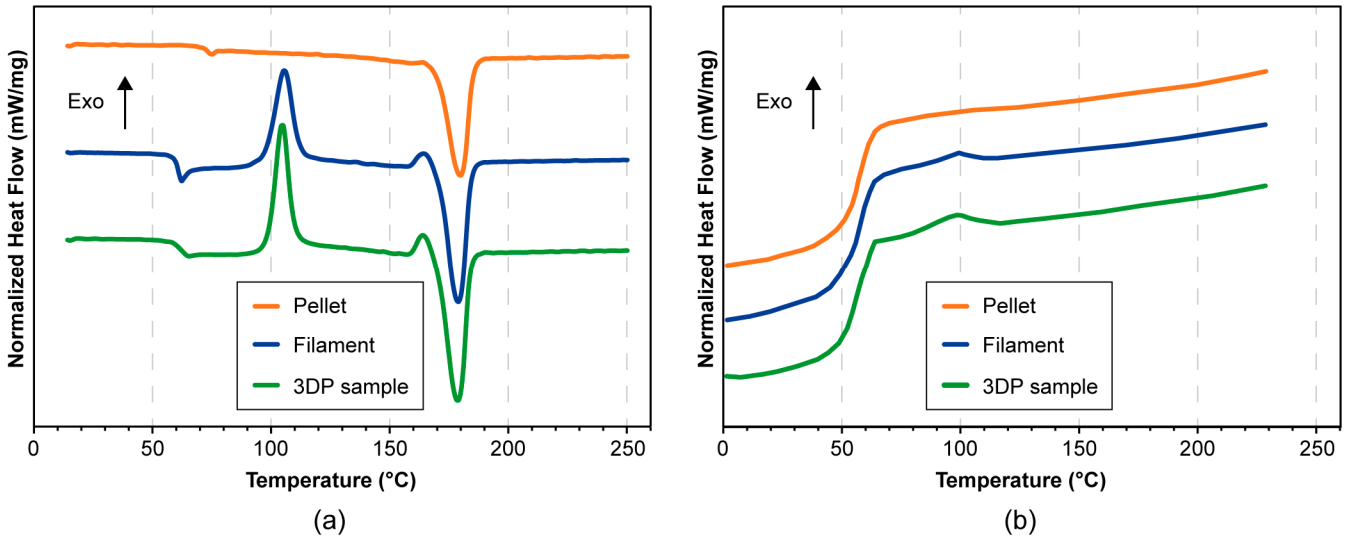

Figure 8. DSC scans during the first heating (**a**) and subsequent cooling (**b**) of three different processed PLA samples.

Comparing the heating scans, no significant variations were observed for the melting temperature, which consistently remained at around 180 °C, in agreement with previously reported values in the literature [30,31,33]. However, a cold crystallization peak appeared during the first heating for both the filament and 3D printed sample. This peak was not detected in the unprocessed PLA pellet. Cold crystallization is the result of thermodynamically unstable states, such as residual stresses, orientations, or imperfect crystal structures, caused by previous cooling conditions [67]. Therefore, the DSC results suggest that during both filament production and 3D printing, the sample cooled too quickly to crystallize properly [68]. The appearance of cold crystallization peaks had a notable effect on the degree of crystallinity, which was approximately 50% for the PLA pellet but then dropped to 9% for the extruded filament and slightly increased to 13.4% for the 3D printed sample. This increase could be attributed to the orientation of the polymer chains during the 3D printing process, which promoted the formation of crystalline structures [69]. The glass transition temperature on the cooling curves remained constant for all three samples. The results of the DSC analyses are summarized in Table 3.

Table 3. Thermal properties of 3D printed PLA samples evaluated by DSC analysis under nitrogen.

	1st Heating					1st Cooling
	T_{cc} (°C)	ΔH_{cc} (J/g)	T_m (°C)	ΔH_m (J/g)	X_c (%)	T_g (°C)
PLA pellet	NA *	NA *	180	46.3	49.8	58
PLA filament	105	33.9	179	42.3	9	59
PLA sample	105	35.5	178	47.9	13.4	59

NA * = Not applicable.

3.4. Tensile Characterization

To characterize the mechanical properties of the 3D printed samples obtained using the self-produced PLA filament, uniaxial tensile tests were carried out using four different infill percentages and two distinct layer heights. Figure 9 presents the main investigated parameters: Young's modulus (E), ultimate tensile strength (UTS), and their specific values (E* and UTS*) normalized relative to the mass of the samples. All data on the tensile characterization are reported in Tables S3–S6 in the Supplementary Materials.

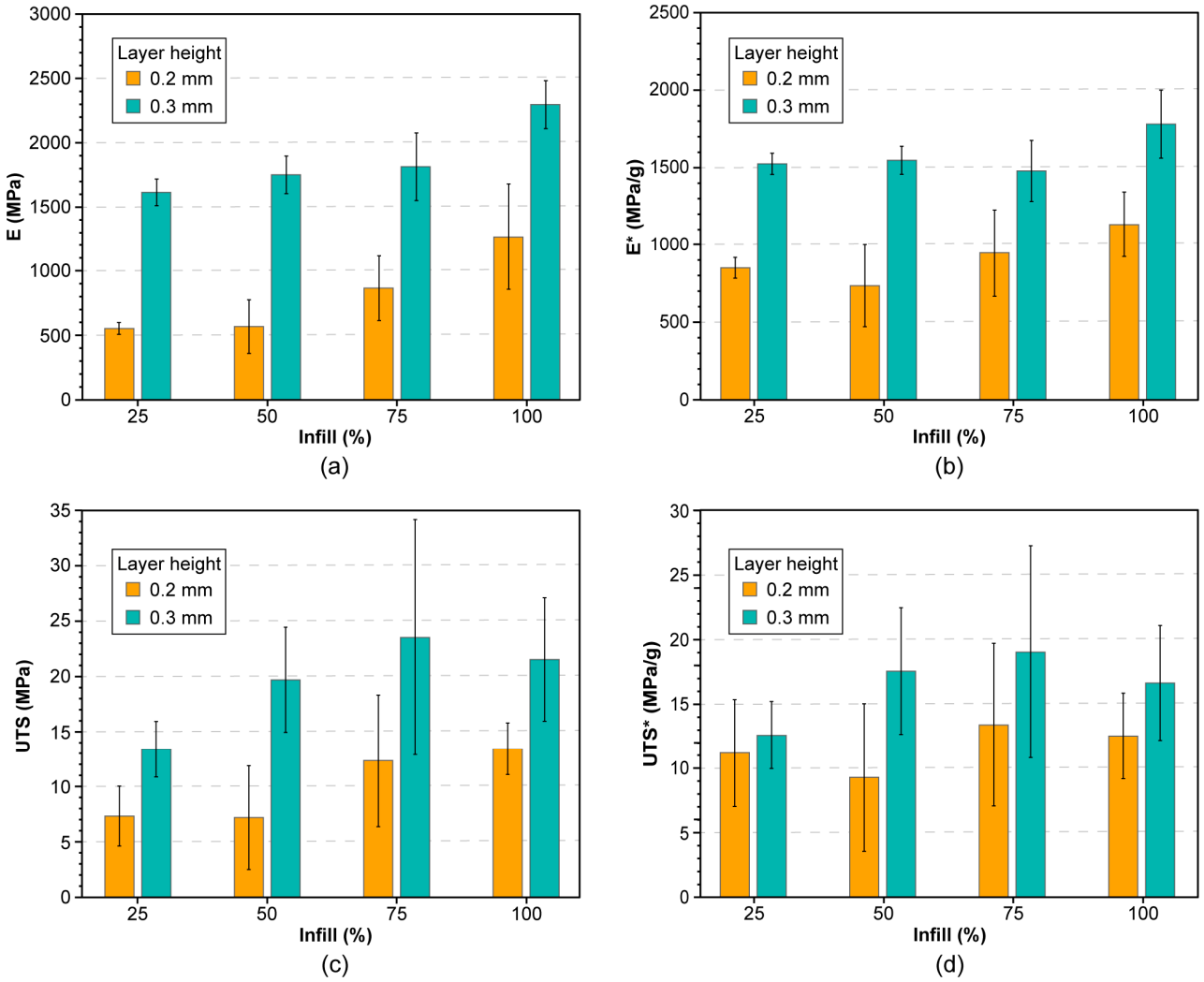

Figure 9. Tensile properties of 3D printed samples obtained by self-produced PLA filament at four different infill percentages (25%, 50%, 75%, and 100%) for two layer heights of 0.2 mm and 0.3 mm: (**a**) Young's modulus (E); (**b**) specific Young's modulus (E*); (**c**) ultimate tensile strength (UTS); (**d**) specific ultimate tensile strength (UTS*).

The average value of E increased with increasing infill percentage. This trend can be attributed to the larger volume of the deposited material. Interestingly, this effect was more pronounced for the 0.2 mm layer height, where E showed a 129% increase between specimens with 25% and 100% infill, whereas E increased by 42% for the 0.3 mm samples from the minimum to the maximum infill percentage (Figure 9a). This consideration is consistent with the fact that the mass of the 0.2 mm samples increased more significantly than that of the 0.3 mm samples (Table 2), which is reflected in the correspondingly more pronounced increase in the Young's modulus. All samples fabricated with a self-produced filament and a 0.3 mm layer height exhibited a stiffer behavior than those 3D printed with a

0.2 mm layer height. This effect was particularly pronounced at low infill percentages (25% and 50%). For example, when confronting the 25% infill samples, the E value increases from 553 MPa to 1616 MPa when the layer height increases from 0.2 mm to 0.3 mm. For 100% infill samples, E shifts from 1269 MPa to 2297 MPa (Figure 9a). To properly interpret these significant variations, two aspects must be considered: the influence of layer height and the specific quality of the 3D printed specimens with the self-produced filament. The influence of the layer height on the mechanical response of the samples aligns with the findings of Rajpurohit et al., who observed higher impact strength with greater layer heights, suggesting that this could be due to stronger interface bonding between layers, which is generated by a greater heat input for thicker layers. Additionally, a higher layer height results in fewer deposited layers, in this case, seven layers for a 0.3 mm layer height versus ten layers for a 0.2 mm layer height. This reduction results in fewer bonding lines and voids between layers, which can enhance mechanical performance [70]. Regarding the specific quality of the 3D printed specimens, it is important to note that the E of 3D printed specimens at low infill percentages (25% and 50%) and a 0.2 mm layer height is significantly lower than the typical values reported for bulk PLA, which generally hovers around 3 GPa [71,72]. This is likely due to poor material deposition and an inconsistent extrusion flow rate during the FFF process, which is caused by inconsistent filament quality used for these specific samples. This hypothesis is supported by the mass calculations presented in Table 2, visual examination in Figure 5(b2), and the standard deviation measured for the self-produced filament.

To gain a better understanding of the behavior of E, its specific value (E*) was also analyzed. At the same infill percentage, E* was consistently higher for the 3D printed samples with a 0.3 mm layer height, although this improvement was approximately half of the increase observed for E (Figure 9b). This smaller improvement supports the notion that the significant increase in E is influenced by the layer height and intrinsic quality of the samples, a factor not considered in E*. Furthermore, since E* does not consider the effect of sample mass, its increase with higher infill percentages was less pronounced than that of E. Specifically, the improvements in E* between the lowest and highest infill percentages were 33% for 0.2 mm samples and 17% for 0.3 mm samples, compared to the much larger increases of 129% and 42% observed for E under the same conditions.

Analyzing Figure 9c,d, it can be appreciated that a layer height of 0.3 mm leads not only to higher stiffness but also to higher UTS and UTS* when compared to samples 3D printed with a 0.2 mm layer height. The maximum average UTS and UTS* values (23.5 MPa and 19 MPa/g, respectively) were registered for samples with a layer height of 0.3 mm and a 75% infill. Both UTS and UTS* exhibited an increasing trend for infill percentages ranging from 25% to 75%, followed by a slight decline for 100% infill. Nonetheless, it should be noted that the highest standard deviation was registered for the 75% infill. For UTS and UTS*, the standard deviation at 75% infill is almost twice the value of other infill percentages.

The tensile test results presented in this work align with those previously reported in the literature [73]. Reference can also be made to the findings of Kechagias et al., where their 3D printed specimens demonstrated a lower E. However, it is important to note that the higher test rate employed by these authors yielded a more reliable response for UTS than for stiffness [38]. Furthermore, from the analysis of the findings, lower strain at break (ε_b) values were consistently observed for higher layer thicknesses (Table 4), regardless of the infill percentage in the 3D printed specimens.

Table 4. Strain at break (ε_b) values of 3D printed samples obtained using self-produced PLA filament at different infill percentages and layer heights.

Layer Height (mm)	0.2				0.3			
Infill Percentage (%)	**25**	**50**	**75**	**100**	**25**	**50**	**75**	**100**
ε_b of specimen 1 (%)	0.97	0.73	3.84	1.40	1.45	1.57	4.03	2.37
ε_b of specimen 2 (%)	3.84	2.53	1.64	1.50	1.74	2.59	2.73	1.29
ε_b of specimen 3 (%)	1.49	1.30	2.36	2.50	2.35	1.93	3.37	2.87
ε_b of specimen 4 (%)	3.72	4.97	4.11	2.83	1.53	2.96	1.17	1.24
ε_b of specimen 5 (%)	3.25	1.38	3.56	2.83	1.39	1.47	1.65	1.63
Mean value (%)	2.65	2.18	3.10	2.21	1.69	2.10	2.59	1.88
Standard deviation (%)	1.33	1.69	1.06	0.71	0.39	0.65	1.18	0.71

3.5. Comparison with 3D Samples Produced with Commercial PLA Filament

To gain a clearer understanding of the previously presented results, eight experimental control sets of samples were first 3D printed using the commercial (C) PLA filament and then characterized to compare the tensile properties with those of the self-produced (SP) filament. As with the SP filament, both layer heights and the four infill percentages were examined. Table 5 summarizes the mass values of the 3D printed tensile specimens obtained using the commercial filament.

Table 5. Masses of the 3D printed specimens with commercial PLA filament classified according to the layer height and infill percentage.

Layer Height (mm)	0.2				0.3			
Infill Percentage (%)	**25**	**50**	**75**	**100**	**25**	**50**	**75**	**100**
Mass of specimen 1 (g)	1.107	1.190	1.275	1.347	1.219	1.241	1.274	1.320
Mass of specimen 2 (g)	1.106	1.194	1.274	1.348	1.221	1.241	1.270	1.316
Mass of specimen 3 (g)	1.106	1.193	1.276	1.349	1.220	1.242	1.269	1.318
Mean value (g)	1.106	1.192	1.275	1.348	1.220	1.241	1.271	1.318
Standard deviation (g)	0.001	0.002	0.001	0.001	0.001	0.001	0.003	0.002

The first and most important observation from the analysis of Table 5 is that the standard deviations for the C filament samples are two to three orders of magnitude lower than the variability observed for the samples produced with the SP filament (Table 2). This suggests that the higher consistency of the C filament diameter, as shown in Figure 5, also results in a much more consistent deposition of material during FFF. For the commercial filament, the average mass of the specimens with the same infill percentage was also higher for a larger layer thickness. However, compared to the SP filament, the mass variation between the specimens printed with the minimum and maximum infill percentages was much smaller, with a difference of 22% for a layer height of 0.2 mm and 8% for a layer height of 0.3 mm.

The comparison of the masses of the specimens 3D printed with the two types of filaments was extended to the actual cross-sectional area. The cross-sectional area analysis was carried out using the X-CT data from the specimens 3D printed with a 0.3 mm layer height at minimum (25%) and maximum (100%) infill percentages. The analysis included 113 transverse cross-sections taken from the middle of the tensile specimen, evenly spaced every 0.25 mm over a total length of 28 mm. The results are summarized in Table 6, and the distribution of the cross-sectional area values is compared using the boxplots in Figure 10.

Table 6. Summary of the cross-sectional area analysis at the center of the tensile specimen over a 25 mm length.

Filament	Commercial (C)		Self-Produced (SP)	
Infill Percentage (%)	**25**	**100**	**25**	**100**
Number of analyzed cross-sections	113	113	113	113
Mean cross-sectional area (mm^2)	9.27	10.01	8.34	9.69
Standard deviation (mm^2)	0.20	0.07	0.20	0.12

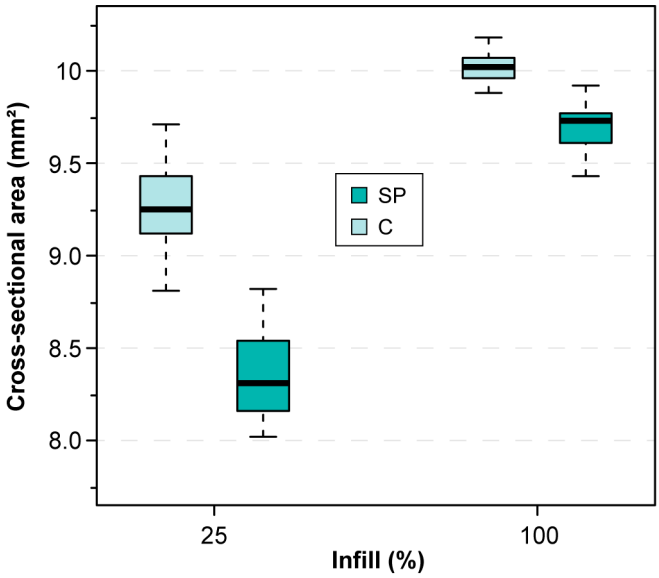

Figure 10. Comparison of the cross-sectional areas of four different samples, categorized by infill percentage (25% and 100%) and filament types (SP and C) for a 3D printing layer height of 0.3 mm.

The analysis confirms that the C specimens contain more deposited material than the SP specimens. The mean cross-sectional area of the C specimens was closer to the nominal value of 10.00 mm^2. Additionally, for both SP and C samples, the cross-sectional area increases with a higher infill percentage (100%) compared with a lower one (25%).

At 25% infill, the SP sample exhibited a lower median cross-sectional area than the C sample (Figure 10), indicating potential structural differences between them. At 100% infill, both the SP and C samples showed larger cross-sectional areas than their 25% infill counterparts, although the C sample still maintained slightly higher values than the SP sample.

The larger variability in the cross-sectional area observed in the specimens with 25% infill can be attributed to the differences in the material distribution along the printing path (Figure 6). Conversely, at 100% infill, both the SP and C samples displayed reduced variability, indicating more consistent cross-sectional areas.

Overall, this analysis highlighted that the infill percentage and filament type significantly affected the cross-sectional area, with potential implications for mechanical strength and structural integrity.

To further evaluate whether and how better deposition of the material during the FFF process reflects on the tensile properties of the specimens, uniaxial tests were conducted on all samples fabricated with the C filament. The main tensile results are illustrated in Figures 11 and 12, whereas all tensile characterization data are reported in Tables S7–S11 of the Supplementary Materials.

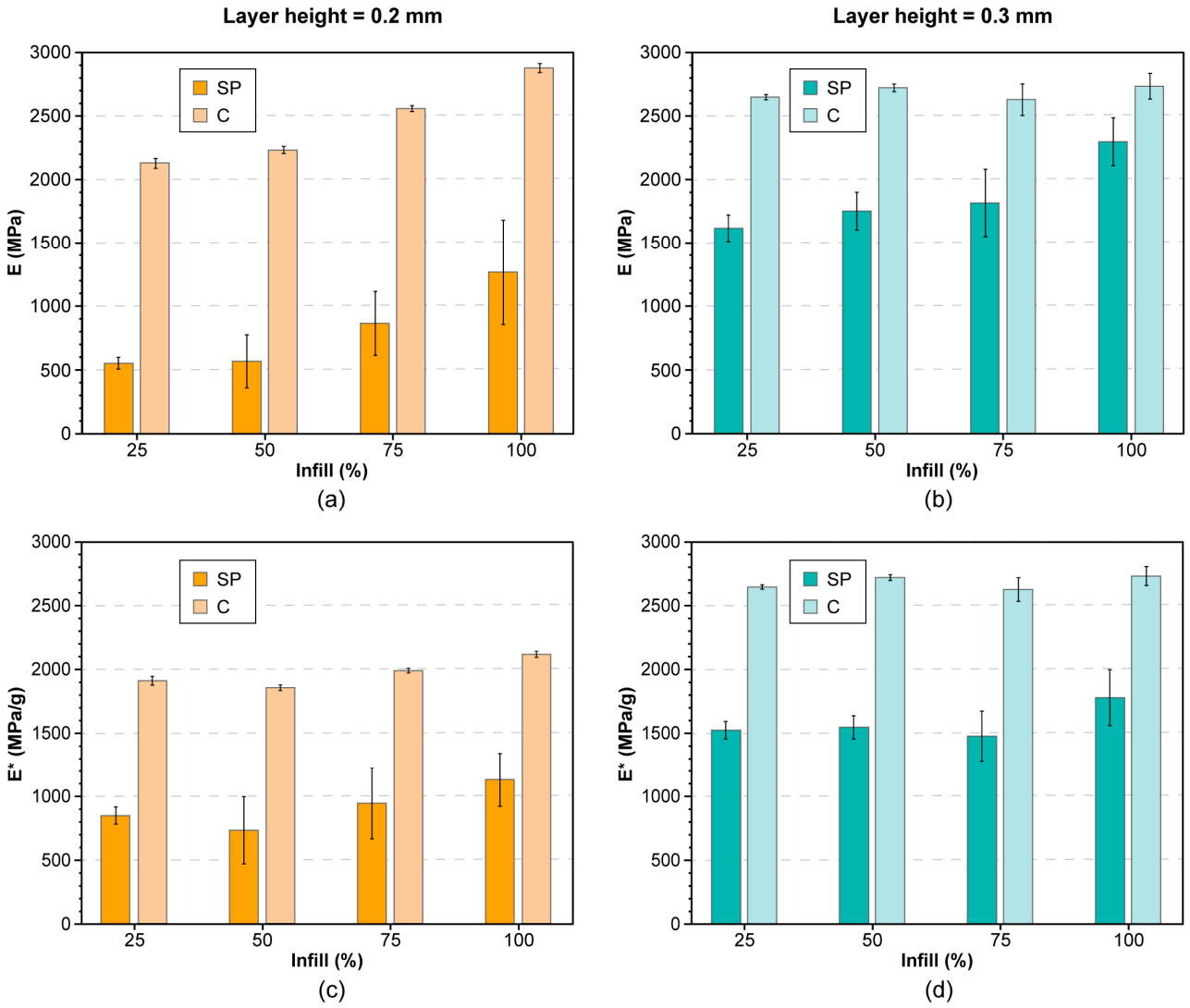

Figure 11. Tensile properties of 3D printed samples fabricated with self-produced (SP) and commercial (C) PLA filaments at four infill percentages (25%, 50%, 75%, 100%): (**a**) Young's modulus (E) of samples printed with a 0.2 mm layer height; (**b**) Young's modulus (E) of samples printed with a 0.3 mm layer height; (**c**) specific Young's modulus (E*) of samples printed with a 0.2 mm layer height; (**d**) specific Young's modulus (E*) of samples printed with a 0.3 mm layer height.

An important observation from Figures 11 and 12 is that the higher variability in the sample mass observed in the SP specimens translates into a broader dispersion of the mechanical results, as reflected by the larger error bars. In contrast, the C samples generally display smaller error bars, indicating better consistency and repeatability of their mechanical properties. Additionally, regardless of the layer height and infill percentage, the samples produced with the C filament consistently exhibited superior mechanical performance in terms of both absolute and specific properties. Notably, similar to the trend observed in the SP samples, the C specimens with a 0.3 mm layer height also exhibited superior mechanical properties (E and UTS) compared to those with a 0.2 mm layer height. This improvement can be attributed to the reduced number of deposited layers. Since the top and bottom layers remain constant, increasing the layer height results in fewer total and infill layers. This structural change may enhance the performance by influencing the overall distribution of stress and interlayer adhesion.

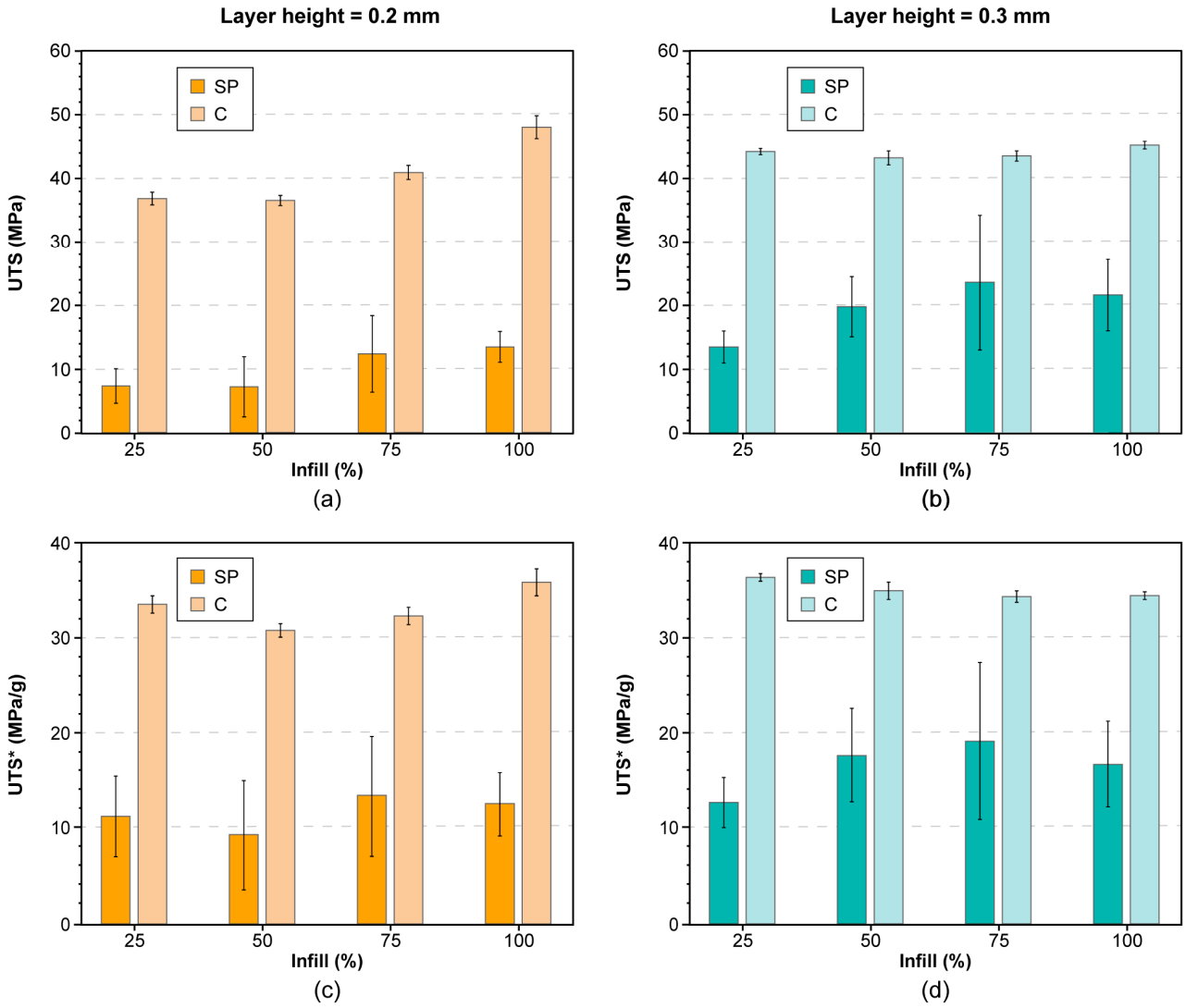

Figure 12. Tensile properties of 3D printed samples fabricated with self-produced (SP) and commercial (C) PLA filaments at four infill percentages (25%, 50%, 75%, 100%): (**a**) ultimate tensile strength (UTS) of samples printed with a 0.2 mm layer height; (**b**) ultimate tensile strength (UTS) of samples printed with a 0.3 mm layer height; (**c**) specific ultimate tensile strength (UTS*) of samples printed with a 0.2 mm layer height; (**d**) specific ultimate tensile strength (UTS*) of samples printed with a 0.3 mm layer height.

The normalized properties, E* and UTS*, followed trends similar to their absolute counterparts, indicating that the improvements in stiffness and strength persist even when accounting for material efficiency. The average values of E* for C samples were 1971 MPa/g and 2125 MPa/g for layer heights of 0.2 mm and 0.3 mm, respectively. In contrast, the SP samples showed significantly lower values of 916 MPa/g and 1583 MPa/g under the same conditions. A similar pattern was observed for UTS*, where C samples achieved 33 MPa/g and 35 MPa/g for 0.2 mm and 0.3 mm layers, respectively, while SP samples reached only 12 MPa/g and 16 MPa/g. The mechanical performance of the commercial filament aligns with the values reported for 3D printed PLA samples in the previous literature [73,74]. The lower mechanical properties of the SP samples, consistent with previous studies on self-produced PLA filaments [35], suggest that commercial filaments provide more reliable structural integrity than self-produced filaments.

To support the experimental tensile test results (Figures 11 and 12), the X-CT data used for the cross-sectional area analysis (Table 6 and Figure 10) were considered in preparing

Figure 13. This figure compares four representative specimens: two fabricated with SP filament and two with C, all 3D printed with a 0.3 mm layer height at both minimum (25%) and maximum (100%) infill percentages. In Figure 13, the middle-plane cross-section of each specimen is highlighted in green, providing a visual representation of its internal structure. Additionally, transversal cross-sections at different positions along the x-axis (−10 mm, −5 mm, 0 mm, +5 mm, +10 mm) within the central narrowed zone of the specimens are depicted.

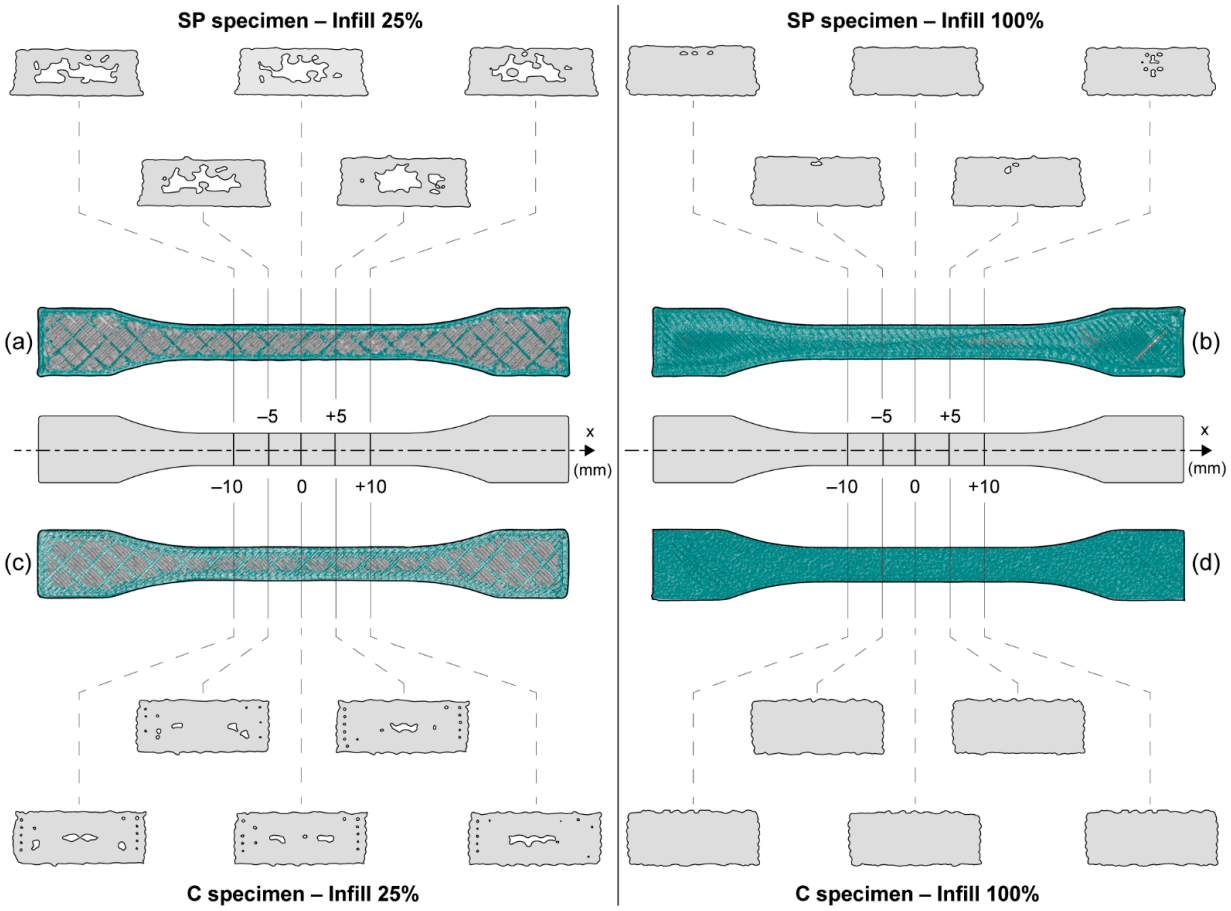

Figure 13. Comparison of material distributions inside different tensile samples fabricated with a layer height of 0.3 mm: 3D printed with 25% infill and self-produced (SP) PLA filament (**a**); 3D printed with 100% infill and self-produced (SP) PLA filament (**b**); 3D printed with 25% infill and commercial (C) PLA filament (**c**); 3D printed with 100% infill and commercial (C) PLA filament (**d**).

At 25% infill, the SP specimen displayed a more irregular internal structure with uneven material distribution (Figure 13a), leading to noticeable voids that result in weaker mechanical properties, especially under tensile stress. In contrast, the C specimen exhibited a more uniform and consistent internal structure at 25% infill, with a smoother material distribution and fewer weak points (Figure 13c).

At 100% infill, the internal structures of both the SP and C specimens appeared significantly more uniform than those of their 25% infill counterparts, with a drastic reduction in internal voids. However, even at 100% infill, the SP specimen still presented minor voids, suggesting small inconsistencies introduced during its manufacturing process (Figure 13b). By contrast, the C specimen maintained a higher degree of internal uniformity at both infill levels (Figure 13c,d), reinforcing its superior mechanical performance, as observed in Figures 11 and 12. Notably, at 100% infill, the C specimen exhibited fully dense cross-sections (Figure 13d).

These structural differences align with the boxplot analysis in Figure 10, where the C specimens exhibited larger and more consistent cross-sectional areas. With 100% infill, both the SP and C specimens demonstrated significantly improved tensile strength compared to the 25% infill versions (Figures 11 and 12). This comparison highlights the significant impact of infill patterns on the mechanical properties of 3D-printed specimens, directly influencing their performance in tensile tests. Consequently, further optimization of the self-production process is necessary to achieve filaments with mechanical performance comparable to that of industrially produced filaments. Improving the reliability of self-produced filaments is crucial for enabling the direct fabrication of end-use components from PLA pellets through 3D printing, paving the way for more sustainable and self-sufficient manufacturing workflows.

Nonetheless, the tensile test results for the 3D printed samples of PLA grade 3D850 align with other studies in the literature for both self-produced [75,76] and commercial filaments [77–79].

Another crucial aspect of filament production that is taken into consideration is energy consumption. The comparison between the commercial PLA filament and the self-produced PLA filament considers only the difference in the filament manufacturing process. The embodied energy required for PLA pellet production and the energy used to produce the tensile specimens remain unchanged. According to the energy consumption data available in databases used for product lifecycle analysis, such as Ansys Granta Selector, the extrusion of 1 kg of PLA pellets requires an average of 5.74 MJ of primary energy. This value is derived from the Granta EduPack 2021 R2 version (Ansys, Inc., Canonsburg, PA, USA) and is slightly higher than that reported in previous versions of the same database [80].

Regarding filament production from pellets using desktop extruders, a study by Enemuoh et al. found that producing approximately 196 g of PLA filament consumed 0.0695 kWh of energy [81]. This equates roughly to 0.355 kWh per kilogram of extruded PLA filament using a Filabot machine. However, to accurately assess primary energy consumption, the primary-to-secondary energy conversion efficiency must be considered. This efficiency typically ranges between 35% and 40%, implying that approximately 3 MJ of primary energy is required for every 1 MJ of electricity.

In line with other studies [82], assuming a primary energy conversion factor of 0.38, the energy consumption for PLA filament extrusion reported by Enemuoh et al. corresponds to 3.36 MJ/kg of filament. In this study, we employed the 3devo extruder, where a total of 0.24 kWh of energy was required to extrude 170 g of the filament. This translates to a secondary energy consumption of 5.06 MJ/kg, which is equivalent to 13.3 MJ/kg of primary energy. When considering only filaments with a consistent diameter suitable for effective 3D printing, the specific energy consumption increases to 17.1 MJ/kg, nearly three times higher than that reported for industrial PLA filament production for FFF (5.74 MJ/kg) [80]. This highlights a significant trade-off between filament quality and energy efficiency during small-scale extrusion. While self-produced filaments offer customization and potential cost savings, further optimization of the extrusion parameters is essential to improve the energy efficiency and competitiveness of commercial alternatives.

4. Conclusions

In this study, a self-produced PLA filament was fabricated using a desktop extruder for application in FFF 3D printing. PLA pellets underwent single-screw extrusion, followed by 3D printing of tensile test specimens with variations in layer height and infill density. The key findings are as follows:

- The SP filament exhibited higher diameter variability, leading to greater deposition rate fluctuations compared to the commercial PLA filament, although 3D printing remained feasible.
- Thermal analysis confirmed that extrusion and printing had no significant impact on the melting and glass transition temperatures of the PLA.
- X-ray computed tomography (X-CT) revealed small voids or imperfections in the cross-sections of the SP samples, indicating inconsistencies in material deposition during 3D printing.
- The resulting uneven material distribution in the SP specimens resulted in inferior mechanical performance compared to that of the C specimens. Tensile testing showed that both stiffness and tensile strength were consistently higher for the C samples than for those printed with the SP filament.
- Using a 0.3 mm layer height improved the efficiency by reducing the specific energy consumption by 50% and increasing the deposition rate by a similar margin. Additionally, specimens printed with this layer height exhibited higher tensile properties than those printed with a 0.2 mm layer height for both the SP and C filaments.
- SP filament exhibited nearly three times higher energy consumption than the C filament, also due to material waste from inconsistent filament diameter.

These findings highlight the need for extrusion parameter optimization to enhance filament quality and printed component performance, ultimately supporting the feasibility of self-produced filaments as a cost-effective and customizable alternative to commercial options. Future research should investigate the correlation between the feedstock filament diameter variability and the deposited material quantity during FFF. This can be achieved through the real-time monitoring of the filament size at the printer's extrusion head and the subsequently deposited layer.

Supplementary Materials: The following supporting information can be downloaded at: https://www.mdpi.com/article/10.3390/jmmp9060172/s1, Table S1: Specific energy consumption (SEC) for the 3D printed PLA samples at different infill percentages and layer heights; Table S2: Deposition rate (DR) for the 3D printed PLA samples at different infill percentages and layer heights; Table S3: Young's modulus (E) for the 3D printed samples with self-produced PLA filament at different infill percentages and layer heights; Table S4: Specific Young's modulus (E*) for the 3D printed samples with self-produced PLA filament at different infill percentages and layer heights; Table S5: Ultimate tensile strength (UTS) for the 3D printed samples with self-produced PLA filament at different infill percentages and layer heights; Table S6: Specific ultimate tensile strength (UTS*) for the 3D printed samples with self-produced PLA filament at different infill percentages and layer heights e; Table S7: Young's modulus (E) for the 3D printed samples with commercial PLA filament at different infill percentages and layer heights; Table S8: Specific Young's modulus (E*) for the 3D printed samples with commercial PLA filament at different infill percentages and layer heights; Table S9: Ultimate tensile strength (UTS) for the 3D printed samples with commercial PLA filament at different infill percentages and layer heights; Table S10: Specific ultimate tensile strength (UTS*) for the 3D printed samples with commercial PLA filament at different infill percentages and layer heights; Table S11: Strain at break (ε_b) for the 3D printed samples with commercial PLA filament at different infill percentages and layer heights.

Author Contributions: Conceptualization, P.M.; Data curation, P.M. and A.G.; Formal analysis, M.S.K. and A.G.; Investigation, L.F. and M.S.K.; Methodology, L.F. and A.G.; Project administration, P.M.; Resources, P.M.; Supervision, P.M.; Validation, A.G.; Visualization, P.M. and A.G.; Writing—original draft, L.F. and A.G.; Writing—review and editing, P.M. and M.S.K. All authors have read and agreed to the published version of the manuscript.

Funding: This study was carried out within the MICS (Made in Italy—Circular and Sustainable) Extended Partnership and received funding from the European Union Next-GenerationEU (Piano

Nazionale di Ripresa e Resilienza (PNRR)—Missione 4 Componente 2, Investimento 1.3—D.D. 1551.11-10-2022, PE00000004). This manuscript reflects only the authors' views and opinions; neither the European Union nor the European Commission can be considered responsible for them.

Data Availability Statement: The original contributions presented in this study are included in the article/Supplementary Materials. Further inquiries can be directed to the corresponding author(s).

Acknowledgments: The authors would like to express their gratitude to their colleague Giovanna Colucci of the DISAT Department for performing the DSC tests.

Conflicts of Interest: All the authors declare that they have no competing financial interests or personal relationships that could have appeared to influence the work reported in this paper.

References

1. Volpini, V.; Giubilini, A.; Corsi, L.; Nobili, A.; Bondioli, F. Characterization of Biocompatible Scaffolds Manufactured by Fused Filament Fabrication of Poly(3-Hydroxybutyrate-*Co*-3-Hydroxyhexanoate). *R. Soc. Open Sci.* **2022**, *9*, 211485. [CrossRef] [PubMed]
2. Kumar, R.; Kumar, M.; Chohan, J.S. The Role of Additive Manufacturing for Biomedical Applications: A Critical Review. *J. Manuf. Process* **2021**, *64*, 828–850. [CrossRef]
3. Ebrahimi, F.; Xu, H.; Fuenmayor, E.; Major, I. Material Compatibility and Processing Challenges in Droplet Deposition Modelling Additive Manufacturing: A Study on Pharmaceutical Excipients Polyvinylpyrrolidone/Vinyl Acetate (PVP/VA) and Polycaprolactone (PCL). *Eur. J. Pharm. Sci.* **2024**, *200*, 106850. [CrossRef]
4. Ebrahimi, F.; Xu, H.; Fuenmayor, E.; Major, I. Tailoring Drug Release in Bilayer Tablets through Droplet Deposition Modeling and Injection Molding. *Int. J. Pharm.* **2024**, *653*, 123859. [CrossRef]
5. Ebrahimi, F.; Xu, H.; Fuenmayor, E.; Major, I. A Comparison of Droplet Deposition Modelling, Fused Filament Fabrication, and Injection Moulding for the Production of Oral Dosage Forms Containing Hydrochlorothiazide. *Int. J. Pharm.* **2023**, *645*, 123400. [CrossRef]
6. Blakey-Milner, B.; Gradl, P.; Snedden, G.; Brooks, M.; Pitot, J.; Lopez, E.; Leary, M.; Berto, F.; du Plessis, A. Metal Additive Manufacturing in Aerospace: A Review. *Mater. Des.* **2021**, *209*, 110008. [CrossRef]
7. Tschorn, J.A.; Fuchs, D.; Vietor, T. Potential Impact of Additive Manufacturing and Topology Optimization Inspired Lightweight Design on Vehicle Track Performance. *Int. J. Interact. Des. Manuf.* **2021**, *15*, 499–508. [CrossRef]
8. Giubilini, A.; Minetola, P. Multimaterial 3D Printing of Auxetic Jounce Bumpers for Automotive Suspensions. *Rapid Prototyp. J.* **2023**, *29*, 131–142. [CrossRef]
9. Gulzar, U.; Glynn, C.; O'Dwyer, C. Additive Manufacturing for Energy Storage: Methods, Designs and Material Selection for Customizable 3D Printed Batteries and Supercapacitors. *Curr. Opin. Electrochem.* **2020**, *20*, 46–53. [CrossRef]
10. Böhme Tillmann and Birtchnell, T. 3DP and the Domestication of Supply Chains in the Future. In *Managing 3D Printing: Operations Management for Additive Manufacturing*; Eyers, D., Ed.; Springer International Publishing: Cham, Switzerland, 2020; pp. 179–190, ISBN 978-3-030-23323-5.
11. Qin, J.; Liu, Y.; Grosvenor, R. A Categorical Framework of Manufacturing for Industry 4.0 and Beyond. *Procedia CIRP* **2016**, *52*, 173–178. [CrossRef]
12. Yadav, A.; Rohru, P.; Babbar, A.; Kumar, R.; Ranjan, N.; Chohan, J.S.; Kumar, R.; Gupta, M. Fused Filament Fabrication: A State-of-the-Art Review of the Technology, Materials, Properties and Defects. *Int. J. Interact. Des. Manuf.* **2022**, *17*, 2867–2889. [CrossRef]
13. Grujovic, N.; Zivic, F.; Zivkovic, M.; Sljivic, M.; Radovanovic, A.; Bukvic, L.; Mladenovic, M.; Sindjelic, A. Custom Design of Furniture Elements by Fused Filament Fabrication. *Proc. Inst. Mech. Eng. C J. Mech. Eng. Sci.* **2017**, *231*, 88–95. [CrossRef]
14. Go, J.; Schiffres, S.N.; Stevens, A.G.; Hart, A.J. Rate Limits of Additive Manufacturing by Fused Filament Fabrication and Guidelines for High-Throughput System Design. *Addit. Manuf.* **2017**, *16*, 1–11. [CrossRef]
15. Corona, B.; Shen, L.; Reike, D.; Rosales Carreón, J.; Worrell, E. Towards Sustainable Development through the Circular Economy—A Review and Critical Assessment on Current Circularity Metrics. *Resour. Conserv. Recycl.* **2019**, *151*, 104498. [CrossRef]
16. Hegab, H.; Shaban, I.; Jamil, M.; Khanna, N. Toward Sustainable Future: Strategies, Indicators, and Challenges for Implementing Sustainable Production Systems. *Sustain. Mater. Technol.* **2023**, *36*, e00617. [CrossRef]
17. Chen, Y. Advantages of 3D Printing for Circular Economy and Its Influence on Designers. *Proc. Des. Soc.* **2022**, *2*, 991–1000. [CrossRef]
18. Ruiz, L.E.; Pinho, A.C.; Resende, D.N. 3D Printing as a Disruptive Technology for the Circular Economy of Plastic Components of End-of-Life Vehicles: A Systematic Review. *Sustainability* **2022**, *14*, 13256. [CrossRef]

19. Despeisse, M.; Baumers, M.; Brown, P.; Charnley, F.; Ford, S.J.; Garmulewicz, A.; Knowles, S.; Minshall, T.H.W.; Mortara, L.; Reed-Tsochas, F.P.; et al. Unlocking Value for a Circular Economy through 3D Printing: A Research Agenda. *Technol. Forecast. Soc. Change* **2017**, *115*, 75–84. [CrossRef]
20. Senyana, L.; Cormier, D. An Environmental Impact Comparison of Distributed and Centralized Manufacturing Scenarios. *Adv. Mat. Res.* **2014**, *875–877*, 1449–1453. [CrossRef]
21. Shaik, Y.P.; Schuster, J.; Shaik, A. A Scientific Review on Various Pellet Extruders Used in 3D Printing FDM Processes. *Open Access Libr. J.* **2021**, *08*, 1–19. [CrossRef]
22. Fico, D.; Rizzo, D.; Casciaro, R.; Esposito Corcione, C. A Review of Polymer-Based Materials for Fused Filament Fabrication (FFF): Focus on Sustainability and Recycled Materials. *Polymers* **2022**, *14*, 465. [CrossRef] [PubMed]
23. Su, J.; Wei Long, N.; Jia, A.; Wai Yee, Y.; Chee Kai, C.; and Sing, S.L. Achieving Sustainability by Additive Manufacturing: A State-of-the-Art Review and Perspectives. *Virtual Phys. Prototyp.* **2024**, *19*, e2438899. [CrossRef]
24. Odera, R.S.; Idumah, C.I. Novel Advancements in Additive Manufacturing of PLA: A Review. *Polym. Eng. Sci.* **2023**, *63*, 3189–3208. [CrossRef]
25. Pan, C.; Gao, Q.; Chen, Y.; Wang, Y.; Tang, Z. Recent Progress in Biosourced Polylactic Acid-Based Biocomposites for Dentistry: A Review. *Int. J. Biol. Macromol.* **2025**, *310*, 143528. [CrossRef]
26. Mohanta, Y.K.; Mishra, A.K.; Lakshmayya, N.S.V.; Panda, J.; Thatoi, H.; Sarma, H.; Rustagi, S.; Baek, K.-H.; Mishra, B. Agro-Waste-Derived Bioplastics: Sustainable Innovations for a Circular Economy. *Waste Biomass Valorization* **2025**. [CrossRef]
27. Tagudin, N.M.F.B.A.; Ibrahim, N.B. Synthesis of Polylactic Acid from Apple, Pineapple, and Potato Residues. *ASEAN J. Chem. Eng.* **2025**, *25*, 75–86. [CrossRef]
28. Cojocaru, V.; Frunzaverde, D.; Miclosina, C.-O.; Marginean, G. The Influence of the Process Parameters on the Mechanical Properties of PLA Specimens Produced by Fused Filament Fabrication&mdash—A Review. *Polymers* **2022**, *14*, 886. [CrossRef]
29. Bardiya, S.; Jerald, J.; Satheeshkumar, V. Effect of Process Parameters on the Impact Strength of Fused Filament Fabricated (FFF) Polylactic Acid (PLA) Parts. *Mater. Today Proc.* **2021**, *41*, 1103–1106. [CrossRef]
30. Ramezani Dana, H.; Ebrahimi, F. Synthesis, Properties, and Applications of Polylactic Acid-Based Polymers. *Polym. Eng. Sci.* **2023**, *63*, 22–43. [CrossRef]
31. Plamadiala, I.; Croitoru, C.; Pop, M.A.; Roata, I.C. Enhancing Polylactic Acid (PLA) Performance: A Review of Additives in Fused Deposition Modelling (FDM) Filaments. *Polymers* **2025**, *17*, 191. [CrossRef]
32. Ilyas, R.A.; Sapuan, S.M.; Harussani, M.M.; Hakimi, M.Y.A.Y.; Haziq, M.Z.M.; Atikah, M.S.N.; Asyraf, M.R.M.; Ishak, M.R.; Razman, M.R.; Nurazzi, N.M.; et al. Polylactic Acid (PLA) Biocomposite: Processing, Additive Manufacturing and Advanced Applications. *Polymers* **2021**, *13*, 1326. [CrossRef] [PubMed]
33. Ebrahimi, F.; and Ramezani Dana, H. Poly Lactic Acid (PLA) Polymers: From Properties to Biomedical Applications. *Int. J. Polym. Mater. Polym. Biomater.* **2022**, *71*, 1117–1130. [CrossRef]
34. Ramezani Dana, H.; El Mansori, M.; Contreras Echevarria, A.; Muñoz Basagoiti, M.X.; Pisarski, M.; Cucuzzella, F.; Sansone, C. Determination of Shear Strength of Additively Manufactured Poly Lactic Acid/Flax Fibre Bio-Composite via the Iosipescu Test. *Compos. Commun.* **2024**, *47*, 101858. [CrossRef]
35. Mirón, V.; Ferrándiz, S.; Juárez, D.; Mengual, A. Manufacturing and Characterization of 3D Printer Filament Using Tailoring Materials. *Procedia Manuf.* **2017**, *13*, 888–894. [CrossRef]
36. Hartig, S.; Hildebrandt, L.; Fette, M.; Meyer, T.; Musienko, E.; Redlich, T.; Wulfsberg, J. Process Parameter Determination for Small Recycling Plants for the Production of Filament for FFF Printing Using the Taguchi Method. *Prog. Addit. Manuf.* **2022**, *7*, 87–97. [CrossRef]
37. Liu, W.; Zhou, J.; Ma, Y.; Wang, J.; Xu, J. Fabrication of PLA Filaments and Its Printable Performance. *IOP Conf. Ser. Mater. Sci. Eng.* **2017**, *275*, 12033. [CrossRef]
38. Kechagias, J.D.; Vidakis, N.; Petousis, M.; Mountakis, N. A Multi-Parametric Process Evaluation of the Mechanical Response of PLA in FFF 3D Printing. *Mater. Manuf. Process.* **2023**, *38*, 941–953. [CrossRef]
39. La Gala, A.; Ceretti, D.V.A.; Fiorio, R.; Cardon, L.; D'hooge, D.R. Comparing Pellet- and Filament-Based Additive Manufacturing with Conventional Processing for ABS and PLA Parts. *J. Appl. Polym. Sci.* **2022**, *139*, e53089. [CrossRef]
40. Fontana, L.; Giubilini, A.; Arrigo, R.; Malucelli, G.; Minetola, P. Characterization of 3D Printed Polylactic Acid by Fused Granular Fabrication through Printing Accuracy, Porosity, Thermal and Mechanical Analyses. *Polymers* **2022**, *14*, 3530. [CrossRef]
41. Trivedi, A.K.; Gupta, M.K.; Singh, H. PLA Based Biocomposites for Sustainable Products: A Review. *Adv. Ind. Eng. Polym. Res.* **2023**, *6*, 382–395. [CrossRef]
42. Wang, P.; Zou, B.; Ding, S.; Huang, C.; Shi, Z.; Ma, Y.; Yao, P. Preparation of Short CF/GF Reinforced PEEK Composite Filaments and Their Comprehensive Properties Evaluation for FDM-3D Printing. *Compos. B Eng.* **2020**, *198*, 108175. [CrossRef]
43. Valente, M.; Sambucci, M.; Rossitti, I.; Abruzzese, S.; Sergi, C.; Sarasini, F.; Tirillò, J. Carbon-Fiber-Recycling Strategies: A Secondary Waste Stream Used for PA6,6 Thermoplastic Composite Applications. *Materials* **2023**, *16*, 5436. [CrossRef]

44. Ghabezi, P.; Sam-Daliri, O.; Flanagan, T.; Walls, M.; Harrison, N.M. Upcycling Waste Polypropylene with Basalt Fibre Reinforcement Enhancing Additive Manufacturing Feedstock for Advanced Mechanical Performance. *Appl. Mater. Today* **2024**, *41*, 102486. [CrossRef]
45. Sam-Daliri, O.; Ghabezi, P.; Steinbach, J.; Flanagan, T.; Finnegan, W.; Mitchell, S.; Harrison, N. Experimental Study on Mechanical Properties of Material Extrusion Additive Manufactured Parts from Recycled Glass Fibre-Reinforced Polypropylene Composite. *Compos. Sci. Technol.* **2023**, *241*, 110125. [CrossRef]
46. Tosto, C.; Bragaglia, M.; Nanni, F.; Recca, G.; Cicala, G. Fused Filament Fabrication of Alumina/Polymer Filaments for Obtaining Ceramic Parts after Debinding and Sintering Processes. *Materials* **2022**, *15*, 7399. [CrossRef] [PubMed]
47. Stanzani, V.; Giubilini, A.; Checchi, M.; Bondioli, F.; Messori, M.; Palumbo, C. Eco-Sustainable Approaches in Bone Tissue Engineering: Evaluating the Angiogenic Potential of Different Poly(3-Hydroxybutyrate-Co-3-Hydroxyhexanoate)–Nanocellulose Composites with the Chorioallantoic Membrane Assay. *Adv. Eng. Mater.* **2023**, *25*, 2200934. [CrossRef]
48. Mohd Pu'ad, N.A.S.; Abdul Haq, R.H.; Mohd Noh, H.; Abdullah, H.Z.; Idris, M.I.; Lee, T.C. Review on the Fabrication of Fused Deposition Modelling (FDM) Composite Filament for Biomedical Applications. *Mater. Today Proc.* **2020**, *29*, 228–232. [CrossRef]
49. Giubilini, A.; Messori, M.; Bondioli, F.; Minetola, P.; Iuliano, L.; Nyström, G.; Maniura-Weber, K.; Rottmar, M.; Siqueira, G. 3D-Printed Poly(3-Hydroxybutyrate-Co-3-Hydroxyhexanoate)-Cellulose-Based Scaffolds for Biomedical Applications. *Biomacromolecules* **2023**, *24*, 3961–3971. [CrossRef]
50. Drummer, D.; Cifuentes-Cuéllar, S.; Rietzel, D. Suitability of PLA/TCP for Fused Deposition Modeling. *Rapid Prototyp. J.* **2012**, *18*, 500–507. [CrossRef]
51. Mohammadi Zerankeshi, M.; Sayedain, S.S.; Tavangarifard, M.; Alizadeh, R. Developing a Novel Technique for the Fabrication of PLA-Graphite Composite Filaments Using FDM 3D Printing Process. *Ceram. Int.* **2022**, *48*, 31850–31858. [CrossRef]
52. Silva, L.R.G.; Bertolim, L.V.; Stefano, J.S.; Bonacin, J.A.; Richter, E.M.; Munoz, R.A.A.; Janegitz, B.C. New Route for the Production of Lab-Made Composite Filaments Based on Soybean Oil, Polylactic Acid and Carbon Black Nanoparticles, and Its Application in the Additive Manufacturing of Electrochemical Sensors. *Electrochim. Acta* **2025**, *513*, 145566. [CrossRef]
53. Kristiawan, R.B.; Imaduddin, F.; Ariawan, D.; Ubaidillah; Arifin, Z. A Review on the Fused Deposition Modeling (FDM) 3D Printing: Filament Processing, Materials, and Printing Parameters. *Open Eng.* **2021**, *11*, 639–649. [CrossRef]
54. Ramezani Dana, H.; El Mansori, M. Investigations on the Mechanical Properties of PLA/Flax Fibre Composites Obtained by Fused Filament Fabrication. *Plast. Rubber Compos.* **2022**, *51*, 393–406. [CrossRef]
55. Domínguez-Robles, J.; Martin, N.K.; Fong, M.L.; Stewart, S.A.; Irwin, N.J.; Rial-Hermida, M.I.; Donnelly, R.F.; Larrañeta, E. Antioxidant PLA Composites Containing Lignin for 3D Printing Applications: A Potential Material for Healthcare Applications. *Pharmaceutics* **2019**, *11*, 165. [CrossRef]
56. *EN ISO 527*; Plastics-Determination of Tensile Properties, Part 1: General Principles. European Committee for Standardization: Brussels, Belgium, 2009.
57. *EN ISO 527*; Plastics-Determination of Tensile Properties, Part 2: Test Conditions for Plastics for Molding and Extrusion. European Committee for Standardization: Brussels, Belgium, 2009.
58. Andersson, H.; Örtegren, J.; Zhang, R.; Grauers, M.; Olin, H. Variable Low-Density Polylactic Acid and Microsphere Composite Material for Additive Manufacturing. *Addit. Manuf.* **2021**, *40*, 101925. [CrossRef]
59. Kohan, M.; Lancoš, S.; Schnitzer, M.; Živčák, J.; Hudák, R. Analysis of PLA/PHB Biopolymer Material with Admixture of Hydroxyapatite and Tricalcium Phosphate for Clinical Use. *Polymers* **2022**, *14*, 5357. [CrossRef] [PubMed]
60. Ambade, V.; Rajurkar, S.; Awari, G.; Yelamasetti, B.; Shelare, S. Influence of FDM Process Parameters on Tensile Strength of Parts Printed by PLA Material. *Int. J. Interact. Des. Manuf. (IJIDeM)* **2025**, *19*, 573–584. [CrossRef]
61. Aly, R.; Olalere, O.; Ryder, A.; Alyammahi, M.; Samad, W.A. Mechanical Property Characterization of Virgin and Recycled PLA Blends in Single-Screw Filament Extrusion for 3D Printing. *Polymers* **2024**, *16*, 3569. [CrossRef]
62. Tamir, T.S.; Xiong, G.; Fang, Q.; Dong, X.; Shen, Z.; Wang, F.-Y. A Feedback-Based Print Quality Improving Strategy for FDM 3D Printing: An Optimal Design Approach. *Int. J. Adv. Manuf. Technol.* **2022**, *120*, 2777–2791. [CrossRef]
63. Gao, X.; Yu, N.; Li, J. Influence of Printing Parameters and Filament Quality on Structure and Properties of Polymer Composite Components Used in the Fields of Automotive. In *Structure and Properties of Additive Manufactured Polymer Components*; Friedrich, K., Walter, R., Soutis, C., Advani, S.G., Fiedler, I., Habil, B., Eds.; Woodhead Publishing Series in Composites Science and Engineering; Elsevier: Amsterdam, The Netherlands, 2020; pp. 303–330, ISBN 978 0 12 819535 2.
64. Cardona, C.; Curdes, A.H.; Isaacs, A.J. Effects of Filament Diameter Tolerances in Fused Filament Fabrication. *IU J. Undergrad. Res.* **2016**, *2*, 44–47. [CrossRef]
65. Minetola, P.; Priarone, P.C.; Ingarao, G. Sustainability for 3DP Operations. In *Managing 3D Printing: Operations Management for Additive Manufacturing*; Eyers, D., Ed.; Springer International Publishing: Cham, Switzerland, 2020; pp. 97–126, ISBN 978 3 030 23323 5.
66. Lunetto, V.; Priarone, P.C.; Galati, M.; Minetola, P. On the Correlation between Process Parameters and Specific Energy Consumption in Fused Deposition Modelling. *J. Manuf. Process* **2020**, *56*, 1039–1049. [CrossRef]

67. Rozwadowski, T.; Noda, H.; Kolek, Ł.; Ito, M.; Yamamura, Y.; Saitoh, H.; Saito, K. Molecular Dynamics and Kinetics of Isothermal Cold Crystallization with Tunable Dimensionality in a Molecular Glass Former, 5′-(2,3-Difluorophenyl)-2′-Ethoxy-4-Pentyloxy-2,3-Difluorotolane. *Phys. Chem. Chem. Phys.* **2023**, *25*, 724–735. [CrossRef]
68. Henricks, J.; Boyum, M.; Zheng, W. Crystallization Kinetics and Structure Evolution of a Polylactic Acid during Melt and Cold Crystallization. *J. Therm. Anal. Calorim.* **2015**, *120*, 1765–1774. [CrossRef]
69. Chen, X.; Kalish, J.; Hsu, S.L. Structure Evolution of A′-Phase Poly(Lactic Acid). *J. Polym. Sci. B Polym. Phys.* **2011**, *49*, 1446–1454. [CrossRef]
70. Rajpurohit, S.R.; Dave, H.K. Impact Strength of 3D Printed PLA Using Open Source FFF-Based 3D Printer. *Prog. Addit. Manuf.* **2021**, *6*, 119–131. [CrossRef]
71. Farah, S.; Anderson, D.G.; Langer, R. Physical and Mechanical Properties of PLA, and Their Functions in Widespread Applications—A Comprehensive Review. *Adv. Drug Deliv. Rev.* **2016**, *107*, 367–392. [CrossRef] [PubMed]
72. Ranakoti, L.; Gangil, B.; Mishra, S.K.; Singh, T.; Sharma, S.; Ilyas, R.A.; El-Khatib, S. Critical Review on Polylactic Acid: Properties, Structure, Processing, Biocomposites, and Nanocomposites. *Materials* **2022**, *15*, 4312. [CrossRef]
73. Wang, S.; Ma, Y.; Deng, Z.; Zhang, S.; Cai, J. Effects of Fused Deposition Modeling Process Parameters on Tensile, Dynamic Mechanical Properties of 3D Printed Polylactic Acid Materials. *Polym. Test.* **2020**, *86*, 106483. [CrossRef]
74. Andronov, V.; Beránek, L.; Krůta, V.; Hlavůňková, L.; Jeníková, Z. Overview and Comparison of PLA Filaments Commercially Available in Europe for FFF Technology. *Polymers* **2023**, *15*, 3065. [CrossRef]
75. Hamat, S.; Ishak, M.R.; Sapuan, S.M.; Yidris, N.; Hussin, M.S.; Abd Manan, M.S. Influence of Filament Fabrication Parameter on Tensile Strength and Filament Size of 3D Printing PLA-3D850. *Mater. Today Proc.* **2023**, *74*, 457–461. [CrossRef]
76. Lau, H.Y.; Hamat, S.; Hussin, M.S.; Manan, M.S.A. Influence of Filament Fabrication Parameter on Mechanical Properties of 3D Printing PLA Filament. *AIP Conf. Proc.* **2024**, *2883*, 040002. [CrossRef]
77. NatureWorks: Ingeo Biopolymer 3D850 Technical Data Sheet. Available online: https://www.natureworksllc.com/~/media/Files/NatureWorks/Technical-Documents/Technical-Data-Sheets/TechnicalDataSheet_3D850_monofilament_pdf.pdf (accessed on 15 May 2025).
78. Torabi, H.; McGreal, H.; Zarrin, H.; Behzadfar, E. Effects of Rheological Properties on 3D Printing of Poly(Lactic Acid) (PLA) and Poly(Hydroxy Alkenoate) (PHA) Hybrid Materials. *ACS Appl. Polym. Mater.* **2023**, *5*, 4034–4044. [CrossRef]
79. Schiavone, N.; Verney, V.; Askanian, H. Effect of 3D Printing Temperature Profile on Polymer Materials Behavior. *3D Print. Addit. Manuf.* **2020**, *7*, 311–325. [CrossRef] [PubMed]
80. Minetola, P.; Eyers, D. Energy and Cost Assessment of 3D Printed Mobile Case Covers. *Procedia CIRP* **2018**, *69*, 130–135. [CrossRef]
81. Enemuoh, E.U.; Menta, V.G.; Abutunis, A.; O'Brien, S.; Kaya, L.I.; Rapinac, J. Energy and Eco-Impact Evaluation of Fused Deposition Modeling and Injection Molding of Polylactic Acid. *Sustainability* **2021**, *13*, 1875. [CrossRef]
82. Lunetto, V.; Galati, M.; Minetola, P.; Priarone, P.C. On the Modelling of the Specific Energy Consumption for the Continuous Fibre Fabrication of Composite Materials. *Prog. Addit. Manuf.* **2024**. [CrossRef]